LBL-33575

ADVANCED FAR INFRARED DETECTORS

E.E. HALLER

Department of Materials Science and Mineral Engineering
University of California

and

ENGINEERING DIVISION
Lawrence Berkeley Laboratory
University of California
Berkeley, California 94720

Proceedings of CIRP-5, Conference on Infrared Physics, Topical Meeting on Infrared Astrophysics, Ascona, Switzerland, June 21-26, 1993; to be published in J. Infrared Physics

MAY 1993

This work was supported in part by NASA interagency grants, US NASA contracts W14606, W16404, W16164 and W17605 through interagency agreement with the US Department of Energy contract DE-AC03-76SF00098.

ADVANCED FAR INFRARED DETECTORS

E.E. HALLER
Lawrence Berkeley Laboratory and
University of California, Berkeley, California 94720, USA

(Received

Abstract

Recent advances in photoconductive and bolometric semiconductor detectors for wavelength 1 mm > λ > 50 μm are reviewed. Progress in detector performance in this photon energy range has been stimulated by new and stringent requirements for ground based, high altitude (airplane and balloon based) and space-borne telescopes for astronomical and astrophysical observations. The paper consists of chapters dealing with the various types of detectors: Be and Ga doped Ge photoconductors, stressed Ge:Ga devices and neutron transmutation doped Ge thermistors. Advances in the understanding of basic detector physics and the introduction of modern semiconductor device technology have led to predictable and reliable fabrication techniques. Integration of detectors into functional arrays has become feasible and is vigorously pursued by groups worldwide.

I. INTRODUCTION

The region of the electromagnetic spectrum ranging from a wavelength of about 1 mm to a few tens of μm holds great promise for a host of exciting discoveries, especially in astronomy and astrophysics. Other fields such as the solid state sciences, biology and medicine also benefit from improvements in detectors for this wavelength range, since these devices are often used in advanced spectroscopies.

There exist a number of reasons why this spectral region poses detection difficulties that are not encountered for much longer or shorter wavelengths. The difficulties are created in part by the black body radiation emitted by ambient temperature instruments and by the warm atmosphere. For astronomical and astrophysical observations there exists the additional problem of the opacity of the atmosphere in much of this spectral region. The former problem can be solved by cooling all the parts of the optical system to low temperatures. The latter problem has led astronomers to locate their instruments at ever higher altitudes, ultimately on satellites orbiting the earth well outside the atmosphere.

Once the background and opacity problems have been solved, the goal is to measure the stream of photons with a noise limitation given by the statistical arrival of photons at the detector.

This brief review will focus on recent advances in the understanding and in the performance of far infrared photon detectors, the actual transducers of photon energy to an electrical signal, working in this wavelength range. The interesting and challenging topic of first stage amplifiers and readout electronics will not be addressed. Because of the relatively small size of the community interested in such detectors, most of the detector research and development has occurred in small groups at Universities and federally funded laboratories. Industry has so far played a relatively minor role. This stands in sharp contrast to the massive industry involvement in the development of infrared detectors for the defense related markets.

The first part of the paper will deal with far infrared extrinsic germanium photoconductors doped with the double acceptor Be (Ge:Be) and the hydrogenic acceptor Ga (Ge:Ga). Uniaxially stressed Ge:Ga photoconductors will also be discussed. The physical operating principles and the technology of photoconductive detectors are very different from those of germanium thermistors which are discussed in the second part of the paper. The former rely on the ionization of dopant impurities in a cold, lightly doped semiconductor followed by free carrier drift motion which constitutes the signal current, while the latter work with the change in hopping conductivity as a function of temperature in strongly doped semiconductors at very low temperatures.

II. EXTRINSIC SEMICONDUCTOR PHOTOCONDUCTORS

1. Detector physics and figures of merit

An extrinsic semiconductor photoconductor consists typically of a small parallelepiped of a semiconductor single crystal which is moderately doped and lightly compensated and has two ohmic contacts (Fig. 1). The crystal is cooled to temperatures low enough for the majority dopants to freeze out. The fundamental operating principles of photoconductors have been understood for some time and a number of reviews treat this topic in detail (1-5). Briefly, the photon detection signal formation is based on three independent events: i) ionization of a majority dopant impurity leading to a free charge carrier, ii) drift motion of the carrier in an externally applied electric field and iii) recombination of the free carrier with an ionized majority impurity. The average distance a free carrier drifts in the photoconductor is related to the average lifetime τ by

$$l = \mu E \tau \qquad (1)$$

with E = electric field strength and μ = mobility. The free carrier drift constitutes a displacement current in the capacitor-like structure of the photoconductor and it appears as the signal current in the external amplifier circuit. The signal current I_S generated by $\dot{N}$ photons per second absorbed through dopant ionization events is

$$I_s = e \dot{N} \eta \, l/L \qquad (2)$$

with e = charge of the electron, η = fraction of photons entering the detector which are absorbed by ionization (also called **responsive quantum efficiency**) and L = interelectrode distance. The ratio l/L is typically called **photoconductive gain** G. Besides the two figures of merit η and G, the **responsivity** R is commonly used to characterize a photoconductor.

$$\begin{aligned} R = I_s/P &= e \dot{N} \eta \, G/\dot{N} h\nu \\ &= e \eta \, G/h\nu \end{aligned} \qquad (3)$$

with P = photon power and $h\nu$ = energy of individual photons.

There exist a number of processes which produce fluctuations (noise) in the photocurrent I_s. The most fundamental fluctuation resides in the quantized nature of the photon stream $(\dot{N})$. The fluctuation in the photon stream arriving at the detector is simply $\sqrt{\dot{N}}$. The ***noise equivalent power*** (NEP) is defined as the photon power required to produce a signal current I_s that is equal to the quadratic sum of all the noise currents in an electrical band width of Δf = 1 Hz:

$$NEP = \left(\sum_i I_{n,i}^2 \, \Delta f \right)^{\frac{1}{2}} / R \qquad (4)$$

In the ideal case only photon related fluctuations contribute to the NEP. This so-called background limited incident photon NEP (NEP_{BLIP}) is found to be:

$$NEP_{BLIP} = \sqrt{2 \left(2 \dot{N}_{total}\right) (h\nu)^2} \qquad (5)$$

The factors of two arise from shot noise associated with the photocurrent and from the distribution in the mean free paths of the individual photogenerated free carriers. Photodiodes and Blocked Impurity Band (BIB) detectors do not exhibit this latter fluctuation and one of the factors of two can be removed from the above equation.

Before closing these brief remarks on basic photoconductor operation, we will introduce one more figure of merit, called **detective quantum efficiency** η_d. The value

of η_d tells us how far the performance of a photoconductor deviates from the ideal performance given by NEP_{BLIP}:

$$\eta_d = \left(\frac{NEP_{BLIP}}{NEP}\right)^2 \qquad (6)$$

In the ideal case η_d approaches unity. In real cases η_d can be very small for unoptimized systems but can reach values 0.4 or higher for well designed systems with state-of-the-art photoconductors. The value of η_d expresses the sum of all noise sources in terms of a hypothetical loss in photon quantum efficiency even though the physical causes for the noise may have a variety of origins which are not related to photon absorption.

When operating photoconductors under a variety of realistic conditions one quickly realizes that the figures of merit defined above can only offer a limited quantitative description of the signal current and the noise. A number of effects which lead to complicated behavior of photoconductive signal currents have been identified and quantitatively understood recently. Modern photoconductors have greatly profited from these results and they no longer display mysterious "spiking" and other uncontrolled effects often seen in older devices.

We will now discuss briefly the effects occurring in the vicinity of modern implanted contacts. For a detailed account the reader is advised to consult the original literature. Modern Ge far infrared semiconductor photoconductors are equipped with two ion implanted and annealed contacts which are typically metalized with a thin palladium adhesion layer (200 Å) and a gold layer (2000-5000 Å). The ion implanted region is doped above the metal-insulator transition concentration by several orders of magnitude. The contact remains a metallically conducting reservoir of free carriers down to the lowest temperatures. The bulk material is doped with a majority dopant (e.g. Ga acceptors) which convert far IR photons into free charge carriers by photoionization of neutral majority dopants. Unavoidably, a small concentration of minority dopants (e.g. P donors) are present. These compensate majority dopants, generating a population of ionized centers equal in concentration to the concentration of the compensating impurities.

A number of attempts have been made to model contacts on low temperature photoconductors. Most of these models were simplified so as to allow analytical solutions. They all dealt with only one contact and an effectively infinite bulk. Unfortunately, these simplifications have limited the general validity of the results in each case. The first complete steady state contact description of a finite device was given by Haegel and White (6). Using a variable finite-difference numerical method these authors calculated the one dimensional dependence of the electric field, the free hole concentration and the ionized acceptor concentration as a function of distance in the near contact region of a Ga acceptor doped Ge photoconductor in the dark and under illumination with and without bias. Haegel and White consider two distinct regions: the metallically doped layer and the lightly doped and compensated bulk region (Fig. 2). The modeling parameters given in Table I are typical for far infrared p-or n-type Ge photoconductors used in low background applications. The relevant processes occur near the contact-bulk interface. Here, free holes are diffusing in a very large hole concentration gradient from the implanted region into the bulk. Some of these holes are captured by acceptors which are ionized because of compensation by the minority donors. Once neutral, these acceptors no longer represent a negative space charge balancing the positive space charge produced by the ionized donors. The ionized donors in turn now set up a space charge related electric field which leads to a hole drift current opposing the diffusion current. Fig. 3 shows the results of this self-consistent model for a 100 μm long Ge:Ga photoconductor which is homogeneously illuminated and under a small bias of 26.3 mV. The optical generation rate is set at 10^{10} holes/s/cm^{-3}, the temperature is 3K and the compensating donor concentration N_{D^+} equals 10^{11} cm^{-3}. The homogeneous illumination raises the free hole concentration in the bulk from a few cm^{-3} to close to 10^4 cm^{-3}. The very rapid increase of the free hole concentration p with distance from the contacts is clearly visible. The complementary reduction in ionized acceptor concentration N_{A^-} extends to a depth of ~ 10 μm. The average electric field in the bulk is

close to 3V cm^{-1}, but crosses to negative values at a distance of 10 μm from the left contact. At the crossing point E=0 V cm^{-1}, the current is given by pure hole diffusion. A reduction of N_D• to 10^{10} cm^{-3} extends these near contact effects to over 30 μm.

Several useful conclusions can be drawn from these calculations. First, we recognize that for state-of-the-art extrinsic germanium photoconductors under typical low background conditions the contact effects reach to distances of at most a few tens of micrometers. For detectors with 500 μm interelectrode distances this poses no problems. However, for very thin detectors with very low minority dopant concentrations it is possible that free carriers spill all the way across the device from one contact to the other. Even without illumination such a detector would not become highly resistive even at very low temperatures and would exhibit excessive dark current, a source of electronic noise. This has recently been verified through experiments on epitaxially grown n^+-n-n^+ Si:P structures. Implanted contacts, however, have been found to be more highly compensated which can limit the carrier spillover effect (7).

Most recently, the authors of the static contact model have extended their work to include the time domain. Using the same modeling parameters as given in Table I, a number of informative results have been obtained. Fig. 4 shows a mesh plot of the free hole concentration increase p/p_0 as a function of position across the detector (linear scale) and as a function of time (logarithmic scale). Time starts at 10^{-10} sec and increases from the front to the back. At 10^{-8} sec the photon flux is increased abruptly by 10%. At the center of the homogeneously illuminated detector the free hole concentration rises to an intermediate plateau within about the free hole lifetime. The highly mobile holes out-diffuse towards the contacts, building up the new steady state space charge distribution. This leads to a roughly parabolic distribution of the hole concentration increase in the early phase of the space charge rearrangements.

After about 1 ms the hole concentration increase begins to rise from the 2% to the final steady state 10% increase. This rise occupies a good fraction of a second for the

specific conditions. It is interesting to follow the change of the external signal current with time. Fig. 5 shows the normalized hole current as a function of time for three fully illuminated photoconductors with different lengths. As the interelectrode distance becomes larger the near contact effects diminish and the long time constant fraction of the signal current becomes smaller. For the longest device (case A) we notice an overshoot reminiscent of the "hook" response frequently observed in older devices. The model calculations allow us to draw several important conclusions. Perhaps the most important one concerns the strong dependence of the long time constant fraction of the signal on the background flux and the interelectrode distance. The response time varies relatively weakly with compensating donor concentration N_D, and with device temperature as long as it is low enough for optical hole generation to exceed thermal ionization of the acceptors.

An interesting test case in which only the central 8% of the device was illuminated with a 10% higher photon flux shows the buildup of an electric dipole field which contains the out diffusion of holes from the illuminated section. The electric fields near the contacts remain unaffected, a clear indication that the contacts themselves are not creating long time constants but that hole diffusion and the establishing of the new space charge distribution dominate the temporal evolution of the signal current.

The results of these very complete device model calculations allow, for the first time, a quantitative evaluation of the effects of all the interacting device operating parameters. This will be most useful in the design of future detectors and detector arrays operating in low background conditions.

2. *Ge:Be Photoconductors*

The optimal spectral response range for extrinsic semiconductor photoconductors is relatively narrow, rising rapidly at the long wavelength cutoff given by the dopant ionization energy (E_c) and falling off with approximately $(E-E_c)^{-3/2}$ to shorter

wavelengths. Fig. 6 shows normalized response curves for stressed Ge:Ga, standard Ge:Ga, Ge:Be and Si:B detectors. Ge:Be photoconductors cover the spectral range gap between Si:B and Ge:Ga devices extending from ~ 30 μm to 50 μm. A significant research and development effort has led to high responsivity, low leakage current Ge:Be detectors (9) and detector arrays (10). The growth of appropriately doped Ge:Be single crystals with low donor compensation was developed approximately ten years ago. Beryllium, a double acceptor in Ge with energy levels at E_v+24.5 meV and E_v+58 meV, poses special doping problems because of its strong oxygen affinity. Using the Czochralski growth method, Ge single crystals were grown from melts contained in either ultra-pure silica or graphite crucibles in a hydrogen or vacuum ambient. The properties of these crystals have been described in detail (3,4,11). Be doping concentrations of 5×10^{14} cm^{-3} to 1×10^{15} cm^{-3} give significant photon absorption in 0.5 to 1 mm thick detectors, while at the same time keeping dark currents caused by hopping conduction at levels as low as a few tens of electrons per second. Individual Ge:Be detectors with responsivities > 10 AW^{-1} at $\lambda = 42$ μm and detective quantum efficiencies $\eta_d \simeq 46\%$ have been reported at low backgrounds (9).

The study and understanding of long time constants particular to Ge:Be devices operated at low temperatures (12) yielded an interesting piece of semiconductor physics. Acceptors in semiconductors with degenerate light and heavy hole bands at the center of the Brioullin zone bind holes with pseudo spin ³/₂ (13). This means that the acceptor 1s ground state has up to four distinct quantum states. Double acceptors such as Be can bind a third hole leading to an overcharged acceptor Be^+. Overcharged donors and acceptors are analogs of a proton binding two electrons (H^-). The binding energy of the third hole for Be acceptors is ~ 4.5 meV. At temperatures < 3 K this binding energy is sufficient to lead to a large number of Be^+ centers in a Ge:Be detector under far infrared illumination. This means that photoionized holes no longer are captured only by Be^- acceptors but also by the neutral Be centers, present at large concentrations, though with a rather small

with a rather small capture cross section because of a lack of Coulomb attraction. Haegel *et al.* (14) presented a quantitative treatment of the effects of Be^+ formation. Long time constants which appear at low temperature were shown to be due to Be^+ formation. At higher operating temperature these effects vanish.

A nice demonstration of Pauli's exclusion principle can be found in uniaxial stress experiments with Ge:Be. The stress splits the valence band degeneracy and the Be double acceptor ground state is described by spin ½ holes. Now, only two holes can occupy the ground state and Be^+ formation is no longer possible. Accordingly, the long time constants disappear in slightly stressed Ge:Be photoconductors (14).

Recent efforts have focused on the development of monolithic Ge:Be arrays. Such arrays will be required for future space borne infrared telescopes such as the Space Infrared Telescope Facility (SIRTF) (15). The most advanced arrays consist of 4×16 pixels, each with a 0.5×0.5 mm^2 area (10). The pixels are 0.625 mm thick and are front illuminated through a transparent, boron implanted contact. The array is currently Indium bump bonded to a sapphire fan-out which connects to warmer electronics. However, plans exist for direct bump bonding to a readout chip, provided the chip can operate at sufficiently low temperatures. Extensive optical and electrical array modeling (16) has yielded very encouraging results regarding cross talk between neighboring pixels for the dimensions given above. It appears that it is not necessary to isolate the individual pixels by cutting deep trenches. The large f-ratio (f=30) of the telescope for which these arrays are developed, the high refractive index of Ge and the dominance of electric field drift motion of the photogenerated charge carriers lead to excellent imaging properties of a close packed array.

3. *Ge:Ga Photoconductors*

Ge:Ga photoconductors are the best low background photon detectors for the wavelength range from ~ 40 μm to 120 μm. Ge:Ga detector physics and technology have

been developed to a very high level of understanding (17). Current efforts focus on a number of rather fundamental open questions and on array development (18,19).

The physical origins of the dark current at low temperatures, an important parameter for very low background applications, are not well understood. Crystals with very similar majority and minority impurity concentrations, dislocation densities and equivalent growth conditions yield photoconductors with dark currents ranging from a few tens to thousands of electrons per second. Experiments are in progress which make use of sophisticated guard ring structures, dislocation free Ge crystals and neutron transmutation doped, isotopically engineered Ge crystals (20) to isolate the sources of excessive dark currents.

A second figure of merit which has been notoriously low is the detective quantum efficiency η_d of Ge:Ga photoconductors. Typical values range from 10% to 20%. No physical mechanisms have been proposed which would explain this large deviation from ideal performance. It is not clear if an actual loss of photons through non-ionizing events or unknown additional noise processes depress the value of η_d. Competing photon absorption processes such as phonon generation are significantly less likely in the photon energy range of Ge:Ga detectors compared to the range covered by Ge:Be devices. Despite this, Ge: Be photoconductors consistently reach higher values of η_d. This finding appears to exclude phonon generation as a major source for the low η_d values for Ge:Ga photoconductors.

Temporary trapping of a photoionized charge carrier followed by re-emission from one of the large number of bound excited states of the primary dopants in the photoconductor may lead to additional noise. Such noise is expected to display a well defined, temperature dependent electrical frequency spectrum.

It should be pointed out that absolute photon flux measurements in the far infrared are notoriously difficult and laborious and only very few accounts of such work have

been published (21). Experiments designed to resolve the low η_d problem will be difficult but definitely worthwhile.

Major efforts currently focus on the development of reliable Ge:Ga detector arrays. The aim is to preserve the excellent characteristics of individual devices and, at the same time, to gain the advantages of arrays. Demonstration arrays of 3×32 pixels of Ge:Ga have been constructed and evaluated (18). These arrays consist of three linear 32 pixel arrays stacked to obtain the second dimension. The performance of the individual pixels was well within the performance range of single Ge:Ga photoconductors. One of the major obstacles in array development is the large operating temperature difference between the photoconductor array working at ~ 1.6 K to 2 K and the readout electronics which requires temperatures above 20 K. In a first attempt the readout electronics was suspended from 25 μm diameter stainless steel wires acting as electrical connections and thermal isolators. For a full 32×32 pixel array a more reliable interconnect scheme is required. Flat multilayer cables of polyamide films and thin metallic conductors offer the excellent thermal, electrical, and mechanical properties required for this task (Fig. 7) (19).

4. Stressed Ge:Ga photoconductors

Application of uniaxial stress along the [100] axis of Ge:Ga crystals reduces the Ga acceptor binding energy, extending the cutoff wavelength λ_c to ~ 240 μm (22). The required forces are rather large and a number of mechanical stress modules have been developed. The fulcrum-flat spring design (Fig. 8) offers convenient variation of the force applied to the detector. Because of the relatively long springs and the small variation of Young's modulus with temperature, the design allows for relatively large mechanical tolerances. A number of groups have developed stressed Ge:Ga photoconductor systems for a wide range of astronomical and astrophysical applications (23,24,25).

Perhaps the biggest challenge for stressed Ge:Ga photoconductors is posed by two dimensional array designs. A successful attempt at constructing a stressed 5×5 Ge:Ga array has been made by Stacey *et al.* (25). In Fig. 9 we show the assembled array, complete with concentrator cones. Each column in the array is assembled as a 5-detector linear array. The detector chips are stacked one on top of the other separated by steel spacers and thin insulator pads. Thin brass contact pads provide the electrical connection. When stress is applied, it translates through the entire stack, providing excellent stress uniformity and eliminating the need for an independent stress mechanism for each chip. The array has been used in a number of high altitude flights with the Kuiper Airborn observatory (KAO) (25).

A major difference in the figures of merit between stressed and unstressed Ge:Ga photoconductors is the large increase in responsivity R in the stressed case. Measured in signal current per photon power, one expects an increase in R when moving to longer wavelength because of the decrease in photon energy. This effect would account for a factor of 2 to 3. We find, however, increases by factors of up to 10. These increases can be traced directly to corresponding increases in free carrier lifetime and mobility. We must assume that the lifetime increases are related to changes in the ground state and the bound excited state spectrum of the Ga acceptors in the stressed Ge. The bound excited states have been studied experimentally (26,27) and theoretically (28,29). Unfortunately, there exists no quantitative approach to correlating lifetime to the acceptor electronic state spectrum. Darken (30) has shown recently that free carrier recombination at low temperatures cannot be explained with the broadly accepted theory of Lax which describes carrier capture by a cascade of phonon emission events transporting the captured carrier from one bound excited state to the next lower one until it arrives in the ground state (31). Quantitative recombination studies which may use pump and probe schemes on short time scales may further the understanding of the experimentally observed lifetime increases.

5. *Future Photoconductor Developments*

The persistent interest in photoconductor arrays which perform to very long wavelengths (λ_c to ~ 250 μm) and do not require mechanical stressing can, at least in principle, be met by two approaches. One path to longer λ_c leads to semiconductors which have very shallow, hydrogenic levels, which is synonymous with very low effective masses. N-type GaAs is by far the best developed semiconductor in this group. Stillmann *et al.* (32) and Gornik (33) have demonstrated long wavelength operation of n-type GaAs photoconductors.

Shallow, hydrogenic donors in GaAs have binding energies of ~ 6 meV and ground state Bohr radii of the order of 80 Å. The large extent of the ground state leads to efficient hopping conduction (i.e., large dark currents) at donor concentrations as low as ~10^{14} cm^{-3} typical for the best bulk GaAs single crystals. On the other hand, large Bohr radii are synonymous with large dipole transition matrix elements between the 1s ground state and the conduction band states. Concentrations of ~10^{12} to 10^{13} cm^{-3} have been shown to lead to efficient photon absorption in 0.1 to 0.5 mm thick photoconductors.

The technological problems associated with the development of high performance n-type GaAs photoconductors are related to the growth of sufficiently pure, low compensation GaAs. Silier *et al.* (34) have successfully grown up to 100 μm thick GaAs layers with N_D–N_A ~10^{12} – 10^{13} cm^{-3} using Liquid Phase Epitaxy (LPE) with liquid Ga as the solvent. We expect that further development of this technique will lead to materials which allow the fabrication of detector arrays sensitive to wavelength near 300 μm (in case transitions to bound excited states are used) and low dark currents.

The second approach to move λ_c to longer wavelength relies on the reduction of the dopant binding energy when a significant wavefunction overlap between neighboring dopant atoms occurs. Such material displays very strong hopping conduction and a high purity blocking layer has to be introduced to reach small dark currents. This idea was

dopant atoms occurs. Such material displays very strong hopping conduction and a high purity blocking layer has to be introduced to reach small dark currents. This idea was first realized with the so-called Blocked Impurity Band (BIB) detectors made from Si:As (35,36). The great success achieved with Si:As BIB arrays has so far not been carried over successfully to Ge BIB devices. Several technological hurdles exist, including the very limited experience with Ge epitaxy and the non-existence of high purity Ge epitaxial growth techniques. Structural defects and impurities continue to affect detector performance (37,38).

A different approach to fabricate Ge BIB detectors which are based on the use of ultrapure Ge doped with ion implantation has led to functional devices which show low leakage currents but exhibit low responsivity because of the rather thin implanted active layer (39,40). It can be expected that continued development efforts together with some new design ideas will lead to functional Ge BIB detectors which can be used in low background astronomical and astrophysical observations.

III. SEMICONDUCTOR THERMISTORS FOR BOLOMETRIC DETECTION

1. General remarks

The physical principles governing photon detection with extrinsic semiconductor photoconductors are very different from those operating in bolometers. The nonequilibrium charge carrier concentration generated through photoionization can easily be made to exceed the dark carrier concentration by cooling the photoconductor to sufficiently low temperatures. Semiconductor thermistors used in bolometric detection, on the other hand, rely on the equilibrium increase in temperature of the crystal lattice caused by photon absorption directly by the crystal or by a separate absorber. The lattice temperature increase leads to an increase of thermally assisted hopping conduction. Modern photoconductors require less cooling than bolometers to reach a desired NEP and

This brief review will focus on neutron transmutation doped (NTD) Ge thermistors which are the temperature to electrical signal converters in bolometers. These devices can now be fabricated reliably with excellent uniformity of all the critical parameters. A large number of NTD Ge bolometer arrays ranging from a few to close to 100 pixels are currently under development at several laboratories. Si thermistors fabricated with microelectronics technologies including lithography and ion implantation have been successfully used in X-ray detection (41). Si thermistor fabrication, however, still suffers from rather large fluctuations in the device parameters. The reasons for these problems lie in the extreme sensitivity of low temperature hopping conductivity to the homogeneity of both majority and minority dopant concentrations. The lowest dopant fluctuations which can be achieved by ion implantation are ~0.5% across a 6" diameter wafer. While such a level of homogeneity is completely sufficient for integrated circuit fabrication, it can pose severe problems for thermistors. At the very low operating temperatures used for the highest performance bolometers, the doping concentrations must be raised to values very close to the metal insulator transition. The resulting sensitivity to even the smallest doping fluctuations is a natural consequence which will be very hard to overcome by trying to improve ion implantation technology. In the following we will show that NTD process leads to very homogeneous doping without special precautions.

A typical modern NTD Ge thermistor consists of a small cube of an appropriately doped NTD Ge crystal. The size may vary from 0.2 to 0.6 mm on edge. Ion implanted contacts on two opposing faces, very similar to the ones described for photoconductors, provide low noise electrical connections. The thickness of the metalization may be reduced such that it does not become the dominant component in the total heat capacity. The cold resistance of the thermistor can be precisely designed, thereby providing the best match for cooled low noise junction field effect transistor amplifiers. In order to take advantage of the excellent uniformity and predictability of NTD Ge bolometer

parameters, great care must be exercised in the mechanical mounting of the thermistor. Due to differences in the thermal expansion coefficients of the materials used, large inhomogeneous stresses can develop in the thermistor crystal. These stresses change the Ge bandstructure, resulting in uncontrolled variations of the dependence of the resistivity on temperature.

2. *Bolometer figures of merit*

The operating principles of bolometers have been described in the literature in detail (42,43,44). If we assume that a constant photon power P_0 and a sinusoidally varying photon power $P\,e^{i\omega t}$ impinge on a bolometer of thermal mass H and with a heat conducting link G, we find the temperature fluctuation amplitude to be

$$\theta_\omega = \eta\, P_\omega \left(G^2 + \omega^2 H^2\right)^{-1/2} \tag{7}$$

with η = fraction of power absorbed. The phase angle φ between P_ω and θ_ω is:

$$\varphi = \tan^{-1} (\omega\, H/G) \tag{8}$$

For $G > \omega\, H$, θ_ω is frequency independent:

$$\theta_\omega = \eta\, P_\omega\, G \tag{9}$$

For semiconductor bolometers there exists an additional source of power provided by the constant biasing current I. The sinusoidally varying part is

$$P_{el} = I^2\, (dR/dT)\, \theta_\omega\, e^{i(\omega t + \varphi)} \tag{10}$$

The temperature coefficient $\alpha = (dR/dt)/R$ is negative for semiconductors, generating an electrical feedback in the bolometer. Mather (43) has shown that this feedback reduces bolometer noise. This effect has been expressed by an effective thermal conductance $G_e = G - I^2\, (dR/dT)$.

The responsivity R is defined as:

$$R = \eta\, I\, \alpha\, R \left(G_e^2 + \omega^2 H^2\right)^{-1/2} \tag{11}$$

In order to independently optimize as many of the above parameters as possible, composite bolometers consisting of an absorber and a thermistor have been developed

(45,46). In the following we will focus on the thermistor part of bolometers. For a comprehensive review of bolometers for far infrared applications the reader is referred to the recent paper by Richards (44).

3. *The Neutron Transmutation Doping (NTD) process and NTD Ge thermistors*

Because of the rise in popularity of NTD Ge thermistors for a variety of applications, we briefly review the basic NTD process. We will show that the process leads to extremely uniform dopant concentrations, a characteristic which has been used for close to twenty years in the fabrication of high power, high voltage Si rectifiers and switches (47). In addition to the excellent uniformity, the NTD process can be controlled to obtain accurate dopant concentrations.

When a stable isotope of an element absorbs a thermal neutron in its nucleus a number of processes may follow. In case the new nucleus is too neutron rich, one of its neutrons will decay into a proton with the emission of an electron and an electronic antineutrino $\bar{\nu}_e$. The beta decay of the isotope ${}^{75}_{32}\mathrm{Ge}$ into ${}^{75}_{33}\mathrm{As}$ is an example:

$$ {}^{74}_{32}\mathrm{Ge} + \mathrm{n} \rightarrow {}^{75}_{32}\mathrm{Ge} \xrightarrow[T_{1/2} = 82.8\ \mathrm{mm}]{\beta^-} {}^{75}_{33}\mathrm{As} + \mathrm{e}^- + \bar{\nu}_e \qquad (12) $$

In relatively few cases a nucleus absorbs an electron from the electron orbits after thermal neutron absorption. Such electron capture (EC) occurs for example in the ${}^{71}_{32}\mathrm{Ge}$ nucleus:

$$ {}^{70}_{32}\mathrm{Ge} + \mathrm{n} \rightarrow {}^{71}_{32}\mathrm{Ge} \xrightarrow[T_{1/2} = 11.2\ \mathrm{d}]{\mathrm{EC}} {}^{71}_{31}\mathrm{Ga} - \mathrm{e}^- + \nu_e \qquad (13) $$

In many cases a stable isotope absorbs a neutron and turns into another stable isotope:

$$ {}^{72}_{32}\mathrm{Ge} + \mathrm{n} \rightarrow {}^{73}_{32}\mathrm{Ge}\,. \qquad (14) $$

While this last example of neutron transmutation is of no interest for semiconductor doping, both the β-decay and the electron capture process lead to new elements shifted by one column in the periodic table of elements away from the column containing the original isotope. In the case of Ge we obtain acceptor and donor dopants in a fixed ratio which is given by the atomic abundance of the individual isotopes and their respective

neutron capture cross sections (48,49). For natural Ge, which is composed of five stable isotopes, we obtain a Ga acceptor concentration of

$$[Ga] = 2.94\times10^{-2}\ cm^{-3}\ per\ neutron/cm^2/s \quad (15)$$

and an As donor concentration of

$$[As] = 8.37\times10^{-3}\ cm^{-3}\ per\ neutron/cm^2/s\ . \quad (16)$$

In addition, a very small concentration of Se double donors is formed which we typically neglect in our calculations.

Because the thermal neutron cross sections depend weakly on the neutron spectrum, one has to calibrate a specific doping position in a nuclear reactor running at a given power. At the Lawrence Berkeley Laboratory we have used the Missouri Research Reactor Facility (50) for processing most of our NTD Ge and we can achieve target concentrations within a few percent.

The major advantages of the NTD process for Ge are quite obvious. Ultra-pure Ge single crystals with doping concentrations $\sim10^{10}\ cm^{-3}$ are commercially available for radiation detector fabrication (51). They are the ideal starting material for NTD. The dopant homogeneity following NTD is extremely high because of the following three facts. First, the stable isotopes have been mixed for very long times and there are no natural forces which separate them. Second, the neutron flux is very homogeneous across small semiconductor slices because of the very large proportions of the reactor core, the source of the neutrons and third, the absorption of thermal neutrons is minimal in 1 to 2 mm thick Ge slices because of the small absorption cross sections, which in turn leads to a uniform neutron exposure throughout the semiconductor. For extreme uniformity the latter factor is the first one to evaluate quantitatively.

The disadvantages of NTD are related to radiation damage by fast neutrons and to the fixed ratio of the acceptor to donor concentration, i.e., the compensation. Careful thermal annealing at 450°C for a few hours under ultra-clean conditions restores the crystalline perfection and activates the As donors (52). The Ga acceptors were shown to

be active in the as-irradiated, unannealed state of NTD Ge. The recent availability of sizable quantities of isotopically enriched Ge has allowed the growth of deliberately mixed isotope crystals with variable compensation ratios (53).

A large body of experimental data for many differently doped NTD Ge samples has accumulated over the past years. Fig. 10 shows a small but representative collection of NTD Ge resistivity data as a function of temperature. Table II contains the neutron fluences and the corresponding dopant concentrations for the individual crystals. A number of groups have contributed their results to this graph. From the results shown in Fig. 10 it becomes clear that the resistivity of NTD Ge can be tailored to a very wide range of values for temperatures ranging from 4 K down to 10 mK or lower.

The resistivity of each NTD Ge sample follows Shklovskii's and Efros' variable range hopping conduction law (54), in some cases over eight orders of magnitude.

$$\rho = \rho_o \exp\left(\Delta/T\right)^{-1/2} \qquad (17)$$

The values for ρ_0 and Δ can be extracted from the data in Fig. 10. Experience shows that accurate temperature measurement with NTD Ge thermistors can be achieved if a number of precautions are taken. First, the mechanical mounting of the crystal to a substrate must be free of mechanical stress. Stress effectively changes the electronic bandstructure of Ge and leads to large changes in ρ_0 and Δ. Second, hot carrier effects must be avoided by using sufficiently small bias currents (55). At very low temperatures (< 50 mK) the free carriers thermally decouple rapidly from the crystal lattice leading to long equilibration time constants and non-linear effects (56).

If the proper precautions are taken, the influence of these effects can be minimized to negligible values all the way down to temperatures of 10 mK and perhaps lower.

4. NTD Ge arrays for sub mm astronomy and astrophysics applications

NTD Ge thermistors have been developed for a broad range of applications. The largest interest in these devices is found currently in submillimeter radioastronomy and astrophysics and in experiments designed to detect dark (or missing) matter in the universe (57,58). Terrestrial telescopes which are or will shortly be equipped with NTD Ge bolometer arrays include, among others, the Institut de Radio Astronomie Millimetrique (IRAM) 30 m submillimeter telescope located in Granada, Spain (59), the 45 m telescope of the Nobeyama Radio Observatory in Japan, the James Clerk Maxwell telescope on Mauna Kea, Hawaii (61), and the sub mm-telescope to be constructed on Mt. Graham, Arizona (59).

The detector arrays which have been developed for these instruments will be used for continuum studies at or near the fundamental background limits which are of the order of $\lesssim 10^{-16}$ W $Hz^{-1/2}$. NTD Ge bolometers operated at temperatures between 100 and 300 mK have demonstrated such background limited performance. First results of the IRAM 30 m telescope with a seven bolometer array are shown in Fig. 11. Superposition of observation maps recorded by the seven element array on the IRAM 30 m telescope has yielded the expected gain of seven in observing time (62).

The most ambitious project is the Submillimetre Common User Bolometer Array (SCUBA) under construction at the Royal Observatory, Edinburgh. SCUBA will be used on the James Clerk Maxwell telescope. Optimistic projections foresee mapping speed improvements of up to 10^4 based on a ten-fold reduction in noise leading to a hundred-fold decrease in integration time and an NTD Ge bolometer array of close to 100 pixels. The large noise reduction is achieved by operating the detectors near 150 mK and by correlation of sky noise between pixels. SCUBA will have two arrays (Fig. 12): a 91 pixel hexagonal assembly for $\lambda = 440$ μm and 350 μm and a 37 pixel assembly for $\lambda = 850$ μm, 750 μm and 600 μm. Simultaneous observations with both arrays are planned.

The design of the bolometer and associated optics consists of a feed horn with $2F\lambda$ opening followed by a circular single mode waveguide. The waveguide leads to the composite bolometer which consists of a bismuth coated sapphire disk on which the $(0.4\ mm)^3$ NTD Ge thermistor is mounted. The thermal conductance is adjusted with fine brass wires. An absorption efficiency of 90% has been measured in tests. The electrical noise evaluation shows that 1/f noise is negligible down to frequencies of 0.5 Hz. This excellent performance can be achieved consistently with ion implanted contacts. The foregoing description of NTD Ge bolometers is specific for SCUBA but most sub mm bolometers used on large terrestrial telescopes use very similar designs. It is quite obvious that for significantly larger arrays some new technology which allows integration should be developed. For reasons described earlier, Si technology faces some very severe difficulties regarding doping uniformities. With the very rapid advances in micro-machined sensors and activators it may become possible to combine the advantages of NTD with integrated circuit technologies.

IV. SUMMARY

Both the physics and technology of semiconductor photoconductors and bolometers have advanced to the point where quantitative performance predictions can be made even for the most stringent applications. We have reviewed far infrared photoconductors consisting of Be and Ga doped Ge which are sensitive in the wavelength range 50 μm to 240 μm and can achieve an NEP < 10^{-17} $WHz^{-1/2}$. Crystal growth and device technology are well understood and quantitative static and dynamic device modeling has been accomplished. Current efforts focus on the development of arrays with up to 1000 pixels preserving the performance of single detectors. These developments will greatly benefit astronomical imaging as well as spectroscopy. A number of interesting questions relating to photocarrier trapping and recombination and the origin of dark currents require answers. The push to sensitivity at longer wavelengths

is addressed by research and development efforts of Ge BIB devices and high purity LPE grown n-type GaAs epitaxial photoconductors.

NTD Ge thermistors used in composite bolometers offer excellent performance down to operating temperatures of tens of mK. At the very lowest temperatures the decoupling of the free charge carriers from the crystal lattice begins to pose problems. NTD Ge thermistors are now widely used in bolometer arrays on sub mm large diameter telescopes. Construction efforts of arrays with close to 100 pixels are in progress promising gains in mapping speeds of up to 10^4. We can expect a great wealth of new exciting data from all the instruments which are currently under construction.

Acknowledgments

A large number of colleagues and collaborators have contributed to the work reported. Foremost, I am indebted to J. Beeman for the assembly of a large number of data from various groups shown in Fig. 10 and for scientific and technical assistance in all the aspects of our photoconductor and thermistor research. W. Hansen has grown many of the ultra-pure and specially doped crystals used for much of the work reviewed. N. Haegel has contributed more than anybody else to the understanding of photoconductor physics and operation. I have learned much in discussions with C. McCreight, P.L. Richards, G. Rieke, C. Townes and many of my former students, too numerous to list. The continuous support from the National Aeronautics and Space Administration has allowed us to develop and understand advanced semiconductor far infrared detectors.

Some of the work reported was supported by NASA interagency grants, US NASA contracts W14606, W16404, W16164 and W17605 through interagency agreement with the US Department of Energy contract DE-AC03-76SF00098.

REFERENCES

1. P. Bratt, in *Semiconductors and Semimetals* Vol. **12**, Chapter 2 , eds. R.R. Willardson and A.C. Beer, Academic Press (1977).

2. E.E. Haller, *Infrared Phys.* Vol. **25**, 257 (1985).

3. N.M. Haegel, M.S. Thesis, Dept. of Mat. Sci. & Min. Eng., University of California, Berkeley, LBL Report #16694 (1983).

4. N.M. Haegel, Ph.D. Thesis, Dept. of Mat. Sci. & Min. Eng., University of California, Berkeley, LBLReport #20627 (1985).

5. N.W. Borgess *et al.*, *NASA Technical Memorandum 78598*, NASA Ames Research Center (1979).

6. N.M. Haegel and A.M. White, *Infrared Phys.* Vol. **29**, 915 (1989).

7. C.S. Olsen, N.M. Haegel, A.M. White, J.E. Huffman, F.F. Kinoshita, and J. Beeman, *Infrared Phys.* **34**, 61 (1993).

8. N.M. Haegel, C.A. Latasa and A.M. White, *Appl. Phys. A.* **56**, 15 (1993).

9. N. M. Haegel, E. E. Haller and P. N. Luke, *Intl. J. Infrared and Millimeter Waves* **4**, No. 6, 945 (1983).

10. M. Scutero, E. T. Young, T. Milner, G. H. Rieke, E. E. Haller, J. Beeman, P. I. Zappella and J. W. Slemmons, SPIE OE/Aerospace Science and Sensing '93, Orlando, FL, April 14-16, 1993, *SPIE Proc.* **1946**, in press.

11. N. M. Haegel and E. E. Haller, "Extrinsic Germanium Photoconductor Material: Crystal Growth and Characterization," presented at Materials Technologies for IR Detectors session of the Third Intl. Symp. on Optical and Optoelectronic Appl. Sci. and Engr., April 14-24, 1986, Innsbruck, Austria. *SPIE Proc.* **659**, 188 (1986).

12. N. M. Haegel and E. E. Haller, *Infrared Phys.* **26**, No. 4, 247 (1986).

13. E. E. Haller, R. E. McMurray, Jr., L. M. Falicov, N. M. Haegel and W. L. Hansen, *Phys. Rev. Lett.* **51**, 1089 (1983); LBL-15988.

14. N. M. Haegel, J. W. Beeman, P. N. Luke, and E. E. Haller, *Phys. Rev. B* **39**, 3677 (1989).

15. G.H. Rieke, M.W. Werner, R.I. Thompson, E.E. Becklin, W.F. Hoffmann, J.R. Houk, F.J. Low, W.A. Stein, and F.C. Witteborn, *Science* Vol. **231**. 807 (1986); see also M.W. Werner and M. Bothwell, Infrared and Submillimeter Astronomy Symposium, COSPAR Congress 1992, to be published in *Advances in Space Research.*

16. T.E. Milner, "The Optical Design of Infrared Detector Arrays", Ph.D. Thesis, Optical Sciences Center, University of Arizona (1992); unpublished.

17. N. M. Haegel, M. R. Hueschen and E. E. Haller, *Infrared Phys.* **25**, 273 (1985).

18. E.T. Young, M. Scutero, G. Rieke, F.J. Low, P. Hubbard, J. Davis, E.E. Haller, and J. Beeman, *Infrared Readout Electronics*, ed. E. Fossum, Proc. SPIE **1684**, 63-74 (1992).

19. E.T. Young, M. Scutero, G.H. Rieke, E.E. Haller, and J.W. Beeman, *Infrared Detectors and Instrumentation*, ed. A.M. Fowler, Proc. SPIE **1946** (1993), in press.

20. Kohei Itoh, W. L. Hansen, E. E. Haller, J. W. Farmer, V. I. Ozhogin, A. Rudnev and A. Thikomirov, *J. Mat. Sci.* (in press).

21. J.-Q. Wang, P.L. Richards, J.W. Beeman, N.M. Haegel, and E.E. Haller, *Appl. Opt.* **25**, 4127 (1986).

22. E. E. Haller, M. R. Hueschen and P. L. Richards, *Appl. Phys. Lett.* **34**, No. 8, 495 (1979).

23. R.W. Russel, G.J. Melnick, G.E. Gull and M. Harwit, *Astrophys. J. Lett.* **240**, L99 (1980).

24. A. Poglitsch, J. W. Beeman, N. Geis, R. Genzel, M. Haggerty, E. E. Haller, J. Jackson, M. Rumitz, G. J. Stacey and C. H. Townes, *Intl. J. Infrared and Millimeter Waves* **12**, 859 (1991).

25. G. J. Stacey, J. W. Beeman, E. E. Haller, N. Geis, A. Poglitsch, and M. Rumitz, *Intl. J. Infrared and Millimeter Waves* **13**, No. 11, 1689-1707 (1992).

26. A. G. Kasanski, P. L. Richards and E. E. Haller, *Appl. Phys. Lett.* **31**, 496 (1977).

27. A. G. Kasanski, P. L. Richards and E. E. Haller, *Solid State Comm.* **24**, 603 (1977).

28. R. Buczko, *Il Nuovo Cimento* **9**, 669 (1987).

29. J. Broeckx and J. Vennik, *Phys. Rev. B* **35**, 6165 (1987).

30. L. Darken, *Phys. Rev. Lett.* **69**, 2839 (1992).

31. B. Lax, *Phys. Rev.* **119**, 1502 (1960).

32. G. Stillman, C.M. Wolfe, and J.D. Dimmock, in *Semiconductors and Semimetals*, Vol. **12**, eds. R.R. Willardson and A.C. Beer, Academic Press (1976).

33. E. Gornik, *Physica* **127B**, 95 (1984).

34. I. Silier, S. Subramanian, E. Diessel, H.-J. Queisser, and E. Bauser, *Appl. Phys. Lett.*, in press.

35. M.D. Petroff and M.G. Stapelbroek, U.S. Patent No. 4568960 (4 Feb. 1986).

36. F. Smulowicz and F.L. Madarasz, *J. Appl. Phys.* **62**, 2533 (1987).

37. Dan M. Watson, Proc. SPIE **1874** (1993), in press.

38. Dan M. Watson, M.T. Guptill, J.E. Huffman, T.N. Krabach, S.N. Raines, and S. Satyapal, submitted to *J. Appl. Phys.*

39. I. C. Wu, J. W. Beeman, P. N. Luke, W. L. Hansen, and E. E. Haller, *Mat. Res. Soc. Proc.* Vol. **216**, 473 (1991).

40. I. C. Wu, J. W. Beeman, P. N. Luke, W. L. Hansen, and E. E. Haller, *Appl. Phys. Lett.* **58**(13), 1431(1991).

41. S.H. Moseley, J.C. Mather, and D. McCammon, *J. Appl. Phys.* **56**, 1257 (1984).

42. E.H. Putley, in *Optical and Infrared Detectors; Topics in Applied Physics* Vol. **19** edited by R.J. Keyes, Springer, New York (1980).

43. John C. Mather, *Applied Optics* **21**, 1125 (1982).

44. P.L. Richards, Review of *Appl. Phys.*, submitted.

45. N.S. Nishioka, P.L. Richards, and D.P. Woody, *Appl. Opt.* **17**, 1562 (1978).

46. A. E. Lange, E. Kreysa, S. E. McBride, P. L. Richards and E. E. Haller, *Intl. J. Infrared and Millimeter Waves* **4**, No. 5, 689 (1983).

47. M.S. Schnoller, *IEEE Trans. Electr. Dev.* **ED-23**, 797 (1976).

48. E. E. Haller, N. P. Palaio, M. Rodder, W. L. Hansen and E. Kreysa, *Proc. Fourth Intl. Conf. on Neutron Transmutation Doping of Semiconductor Materials*, National Bureau of Standards, June 1-2, 1982, Gaithersburg, MD, ed. R.D. Larrabee, Plenum Press, p. 21-36 (1984).

49. N. P. Palaio, M. Rodder, E. E. Haller and E. Kreysa, *Intl. J. Infrared and Millimeter Waves* **4**, No. 6, 933 (1983).

50. Research Reactor Facility, Research Park, Columbia, Missouri 65211

51. W. L. Hansen and E. E. Haller, Proc. Mat. Res. Soc. 1982 Annual Meeting, Symposium F, Nuclear Radiation Detector-Materials, eds. E.E. Haller, H.W. Kraner and W.A. Higinbotham, Elsevier Science Publishing Co., Inc., New York, *Mat. Res. Soc. Proc.* Vol. **16**, p. 1-16 (1983).

52. I. S. Park and E. E. Haller, *J. Appl. Phys.* **64**, 6775 (1988).

53. K. Itoh, W. L. Hansen, E. E. Haller, J. W. Farmer and V. I. Ozhogin, *Proc. of The 5th Intl. Conf. on Shallow Impurities in Semiconductors: Physics and Control of Impurities*, ed. T. Taguchi, Materials Science Forum **117 & 118**, 117 (1993).

54. B.I. Shklovskii and A.L. Efros, in *Electronic Properties of Doped Semiconductors*, Solid State Series Vol. **45**, Springer-Verlag, Berlin (1984).

55. T. W. Kenny, P. L. Richards, I. S. Park, E. E. Haller and J. Beeman, *Phys. Rev. B* **39**, 8476 (1989).

56. N. Wang, F. C. Wellstood, B. Sadoulet, E. E. Haller and J. Beeman, *Phys. Rev. B* **41**, 3761 (1990).

57 T. Shutt, N. Wang, B. Ellman, Y. Giraud-Heraud, C. Stubbs, P. D. Barnes, Jr., A. Cummings, A. Da Silva, J. Emes, E. E. Haller, A. E. Lange, R. R. Ross, B. Sadoulet, G. Smith, W. Stockwell, S. White, B. A. Young, and D. Yvon, *Phys. Rev. Lett.* **69**, 3425 (1992).

58. T. Shutt, B. Ellman, P. D. Barnes, A. Cummings, A. Da Silva, J. Emes, Y. Giraud-Heraud, E. E. Haller, A. E. Lange, R. R. Ross, J. Rich, B. Sadoulet, G. Smith, W. Stockwell, C. Stubbs, N. Wang, S. White, B. A. Young, and D. Yvon, *Phys. Rev. Lett.* **69**, 3531 (1992).

59. E. Kreysa, E.E. Haller, H.-P. Gmünd, G. Haslam, R. Lemke, and A. Sievers, *Proc. 4th Intl. Conf. on Space Terahertz Technology*, Univ. of California, Los Angeles, 3/30-4/1/93.

60. N. Kuno, H. Matsuo, Y. Mizumoto, A. E. Lange, J. W. Beeman and E. E. Haller, subm. to *Intl. J. Infrared and Millimeter Waves*, (1993).

61. C.R. Cunningham and W.K.P. Gear, *Proc. SPIE: Instrumentation in Astronomy VII* **1235**, 515 (1990).

62. E. Kreysa, *Proc. Intl. Symp. of Photon Detectors for Space Instrumentation*, ed. T.D. Guyenne, ESA/ESTEC Noordwijk (1993), in press.

63. J. Q. Wang, P. L. Richards, J. W. Beeman and E. E. Haller, *Appl. Opt.* **26**, 4767 (1987).

Table I. Modeling parameters for Ge:Ga detectors

Acceptor concentration, N_A	2×10^{14} cm^{-3}
Donor concentration, N_D	$10^{14} - 10^{12}$ cm^{-3}
Mobility (T = 3 K), μ	3×10^5 cm^2/Vs
Capture cross section (T = 3 K), σ	10^{-11} cm^2
Thermal hole velocity (T = 3 K), v	2×10^6 cm/s
Static dielectric constant, ϵ_s	1.4×10^{-12} F/cm
Acceptor ionization energy	11.3 meV

Table II. NTD Ge thermistor data

NTD#	n Dose (cm^{-2})	N_{Ga} (cm^{-3})	N_{As} (cm^{-3})	N_{Se} (cm^{-3})	$N_{Ga} - \Sigma N_D$(cm^{-3})
4	3.38E+17	9.94E+15	2.83E+15	1.86E+14	6.74E+15
5	7.50E+17	2.21E+16	6.29E+15	4.13E+14	1.50E+16
13	1.24E+18	3.65E+16	1.04E+16	6.83E+14	2.47E+16
15	1.54E+18	4.53E+16	1.29E+16	8.49E+14	3.07E+16
16	2.07E+18	6.09E+16	1.73E+16	1.14E+15	4.13E+16
18	2.61E+18	7.67E+16	2.19E+16	1.44E+15	5.20E+16
26	2.82E+18	8.29E+16	2.36E+16	1.55E+15	5.62E+16
28	3.07E+18	9.03E+16	2.57E+16	1.69E+15	6.11E+16
12	3.33E+18	9.79E+16	2.79E+16	1.83E+15	6.64E+16
25	4.20E+18	1.23E+17	3.52E+16	2.31E+15	8.37E+16

Figure Captions

Fig. 1 Schematic of a p^+-p-p^+ semiconductor photoconductor. At low temperatures the uncompensated acceptors are frozen out, i.e., neutral (A^o). Incoming photons can ionize neutral acceptors forming a free hole ($\oplus$) and a negatively charged acceptor (A^-). The free hole drifts an average distance l before it recombines with an A^-.

Fig. 2 The near-contact band diagram showing the Fermi level position relative to the valence band edge. (Courtesy Haegel and White, Ref. 6)

Fig. 3 The free hole concentration (P), the ionized acceptor concentration(A^-) and the electric field in a lightly biased (V=26.3 mV) p^+-p-p^+ Ge:Ga photoconductor which is homogeneously illuminated. (Courtesy Haegel and White, Ref. 6)

Fig. 4 Mesh plot of the relative free hole increase as a function of position and time in a homogeneously illuminated p^+-p-p^+ Ga:Ge photoconductor. The illumination is turned on at 10^{-8} s. (Courtesy Haegel *et al.*, Ref. 8)

Fig. 5 Hole current as a function of time for three Ge:Ga photoconductors with lengths A) 200 μm, B) 100 μm, and C) 40 μm for constant illumination. (Courtesy Haegel *et al.*, Ref. 8)

Fig. 6 Schematic relative response of Si:B, Ge:Be, Ge:Ga and uniaxially stressed Ge:Ga photoconductors.

Fig. 7 Tape automated bonding focal plane module of the integrator and multiplexer chips for a linear 32 pixel Ge:Ga array. The Ge:Ga photoconductors are connected to the chip by the 32 wires leading to the left. The readout and power wires come from the right. (Courtesy Young *et al.*, Ref. 19)

Fig. 8 Stress rig for uniaxially stressing Ge:Ga, a: adjusting screw, b: flat springs, c: fulcrum, d: body, e: fulcrum holding pin, f: Ge:Ga photoconductor,

g: stressing pistons, h: detector positioning screw. (Courtesy Wang *et al.*, Ref. 63)

Fig. 9 Completed 5×5 stressed Ge:Ga array with light collecting cones. (Courtesy Stacey *et al.*, Ref. 25)

Fig. 10 Logarithm of the resistivity as a function of $T^{-1/2}$ for ten selected NTD Ge crystals. The neutron dose and the resulting dopant concentrations are listed in Table II. (Courtesy J. Beeman, Lawrence Berkeley Laboratory)

Fig. 11 Beam pattern of the seven bolometer array obtained on Uranus with the IRAM 30 m telescope. Contour levels are in percent of peak intensity. (Courtesy Kreysa *et al.*, Ref. 59)

Fig. 12 The SCUBA 91 pixel and 37 pixel NTD Ge bolometer arrays under development for the James Clerk Maxwell submillimeter telescope. (Courtesy Cunningham and Gear, Ref. 61)

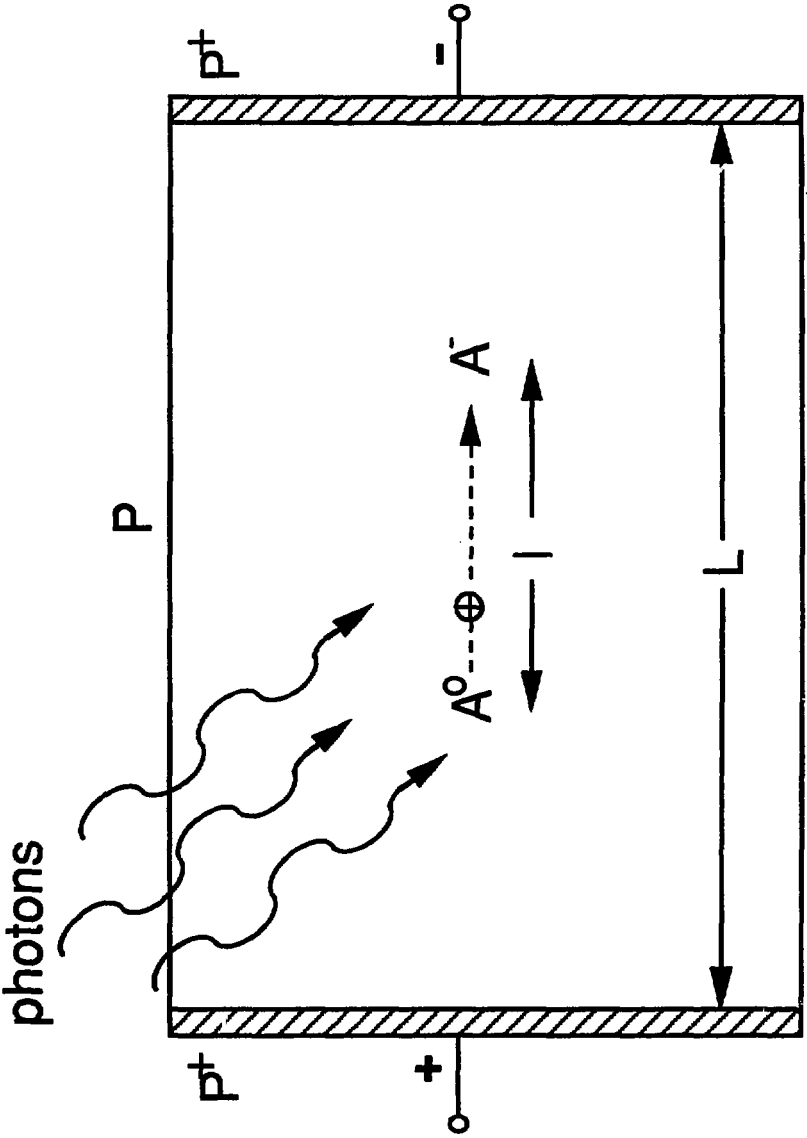

XBL 935-644

Fig. 1

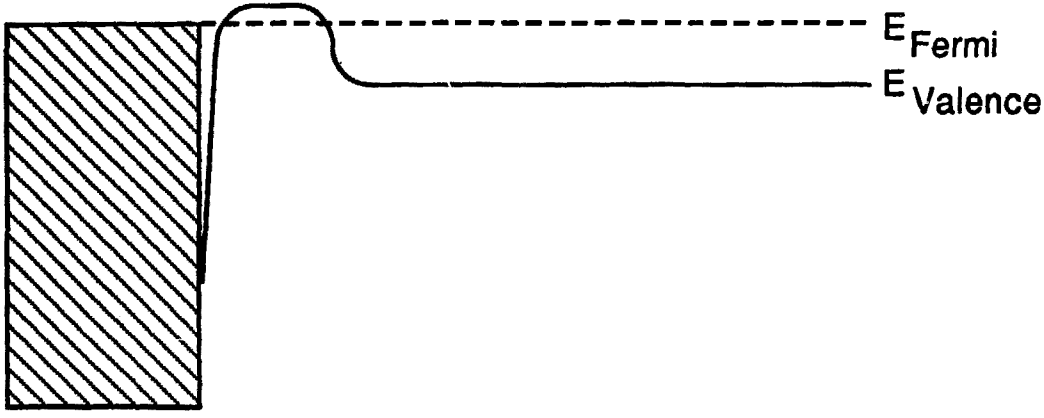

XBL 935-643

Fig. 2

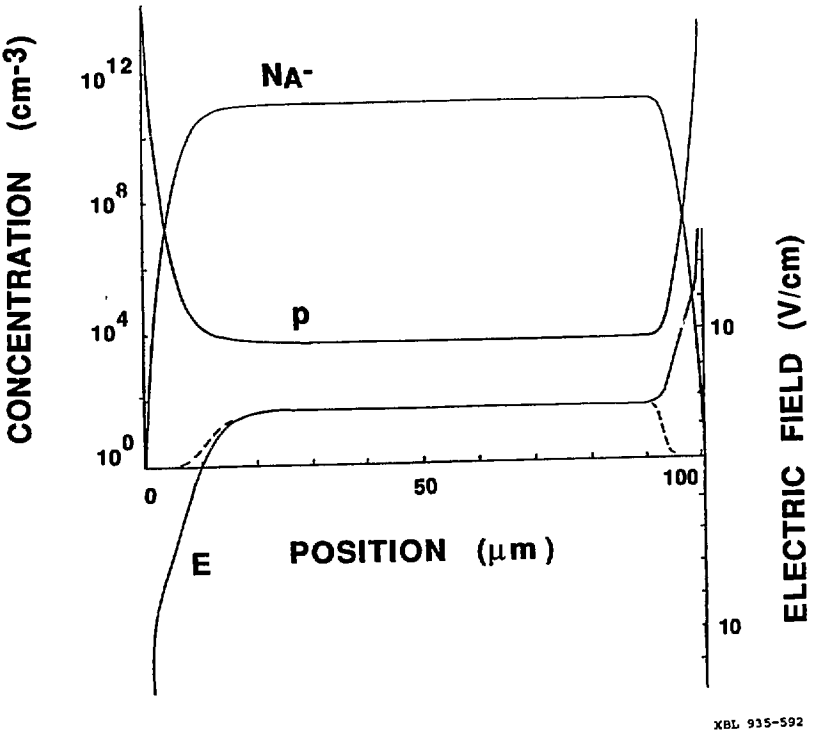
CONCENTRATION (cm-3)
10^12
10^8
10^4
10^0
NA-
p
E
0
50
100
POSITION (μm)
10
10
ELECTRIC FIELD (V/cm)
XBL 935-592

Fig. 3

P/Po (A.U.)
1.10
1.08
1.06
1.04
1.02
1.00
Position (microns)
35 30 25 20 15 10 5 0 -5 -10
Time (msec)
1 0 -1 -2 -3 -4 -5 -6 -7 -8 -9 -10
XBL 935-591

Fig. 4

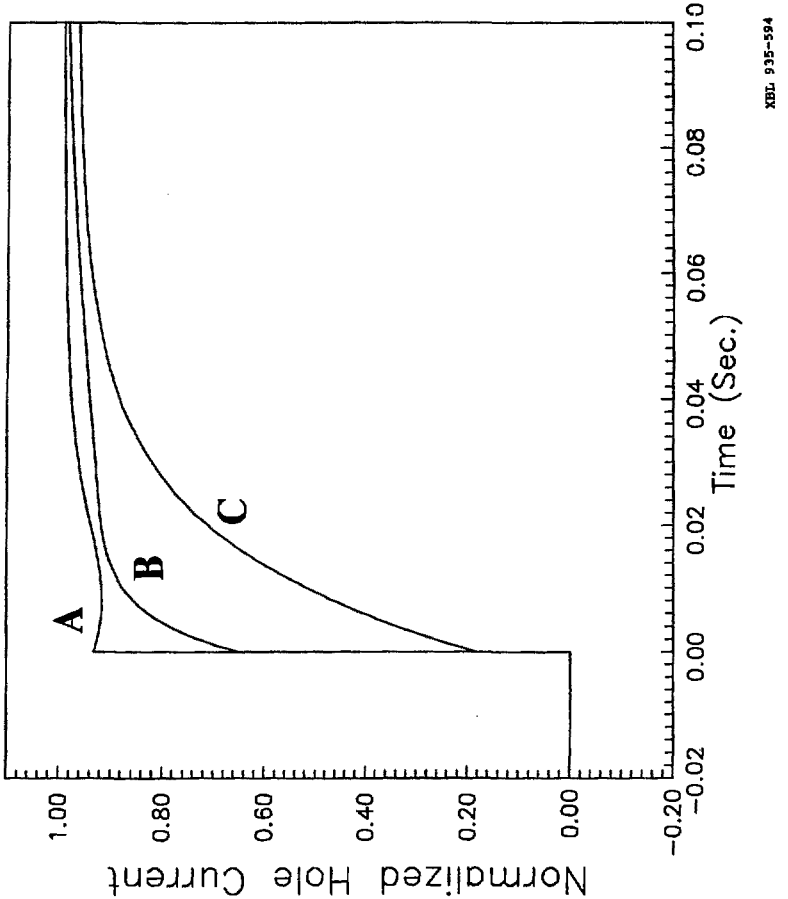
Normalized Hole Current
1.00
0.80
0.60
0.40
0.20
0.00
−0.20
−0.02
0.00
0.02
0.04
0.06
0.08
0.10
Time (Sec.)
A
B
C
XBL 935-594

Fig. 5

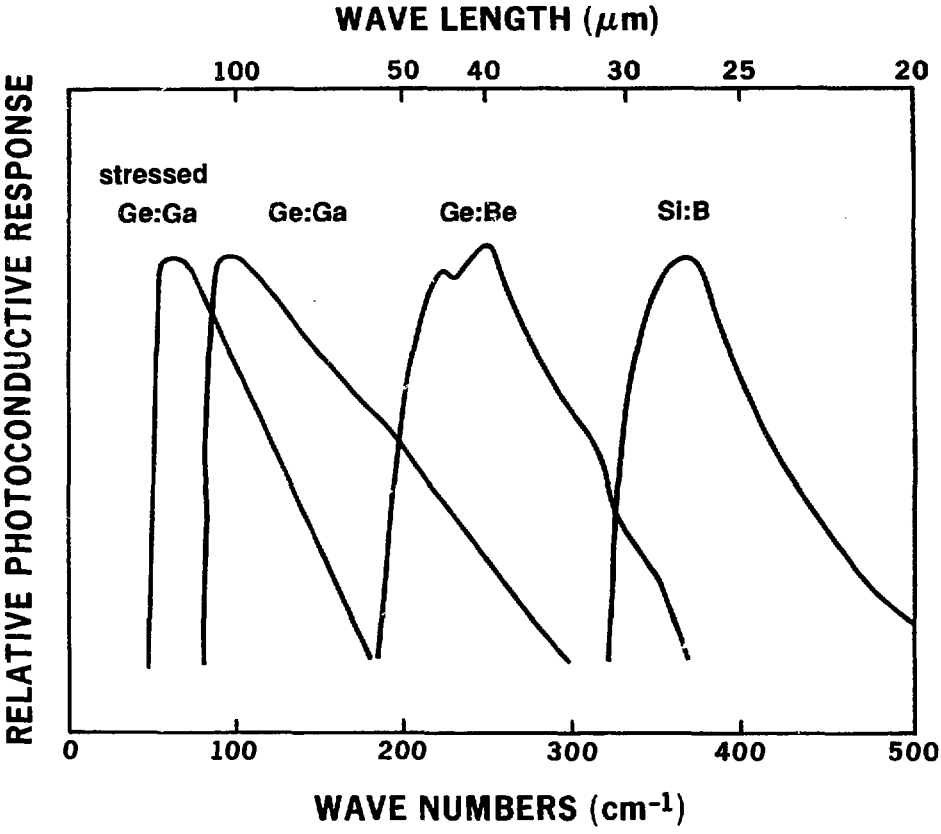

XBL 935-642

Fig. 6

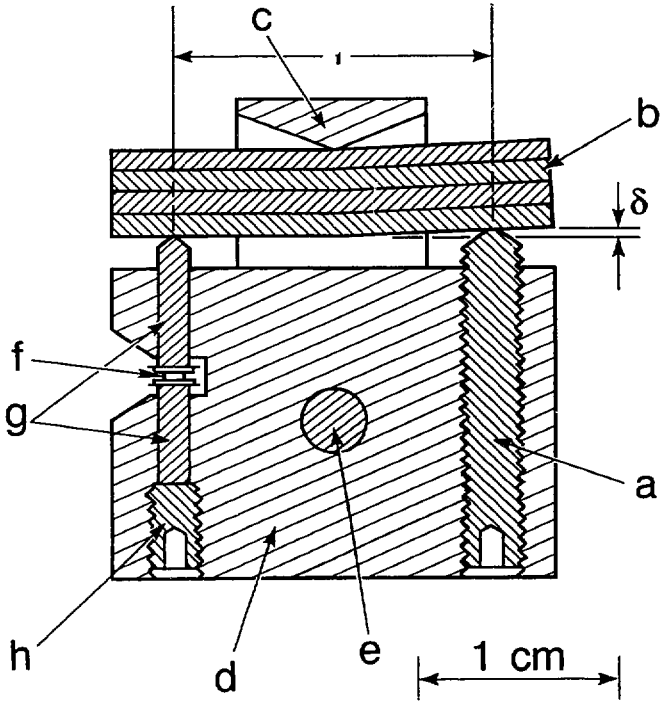

XBL 8611-6483

Fig. 8

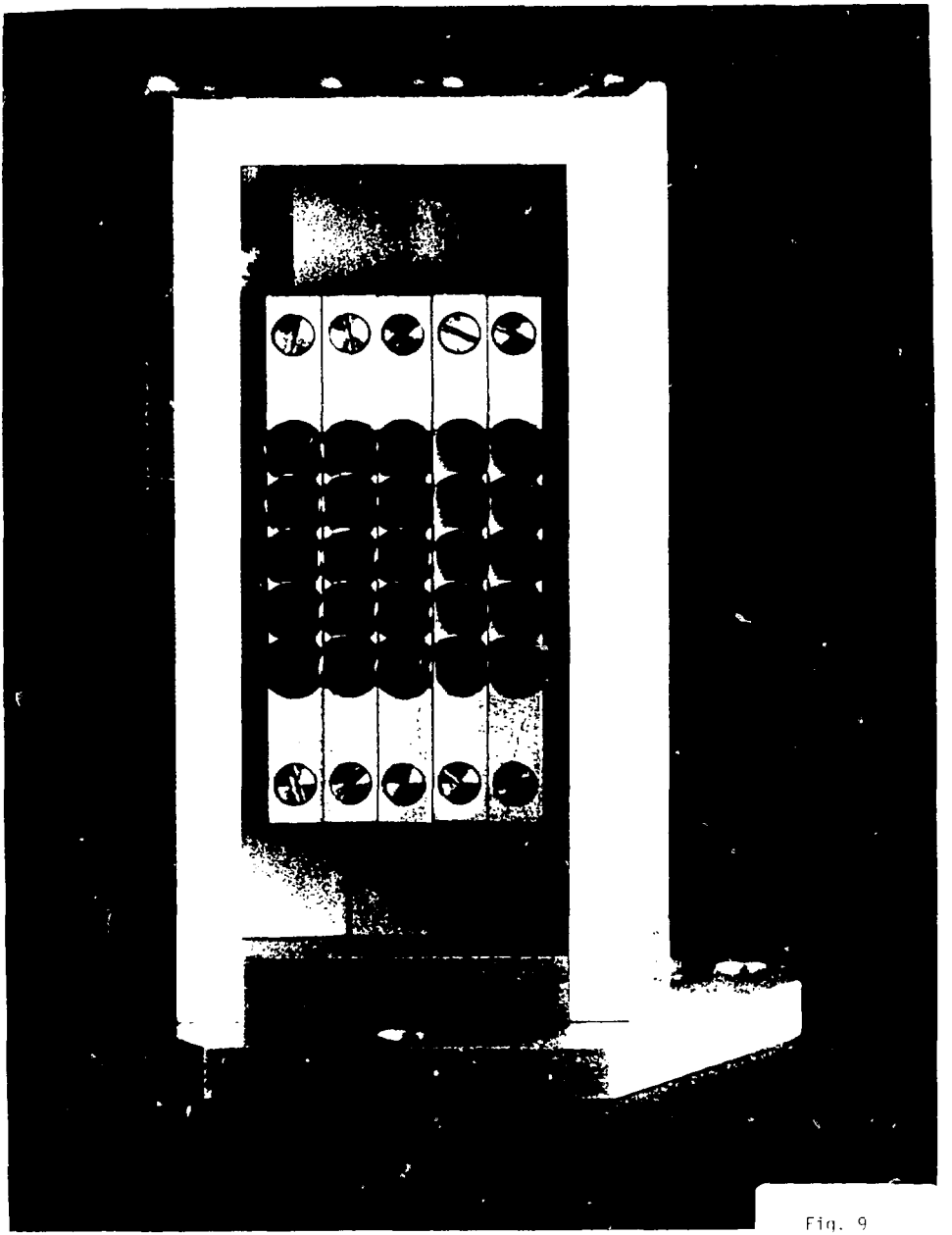

Fig. 9

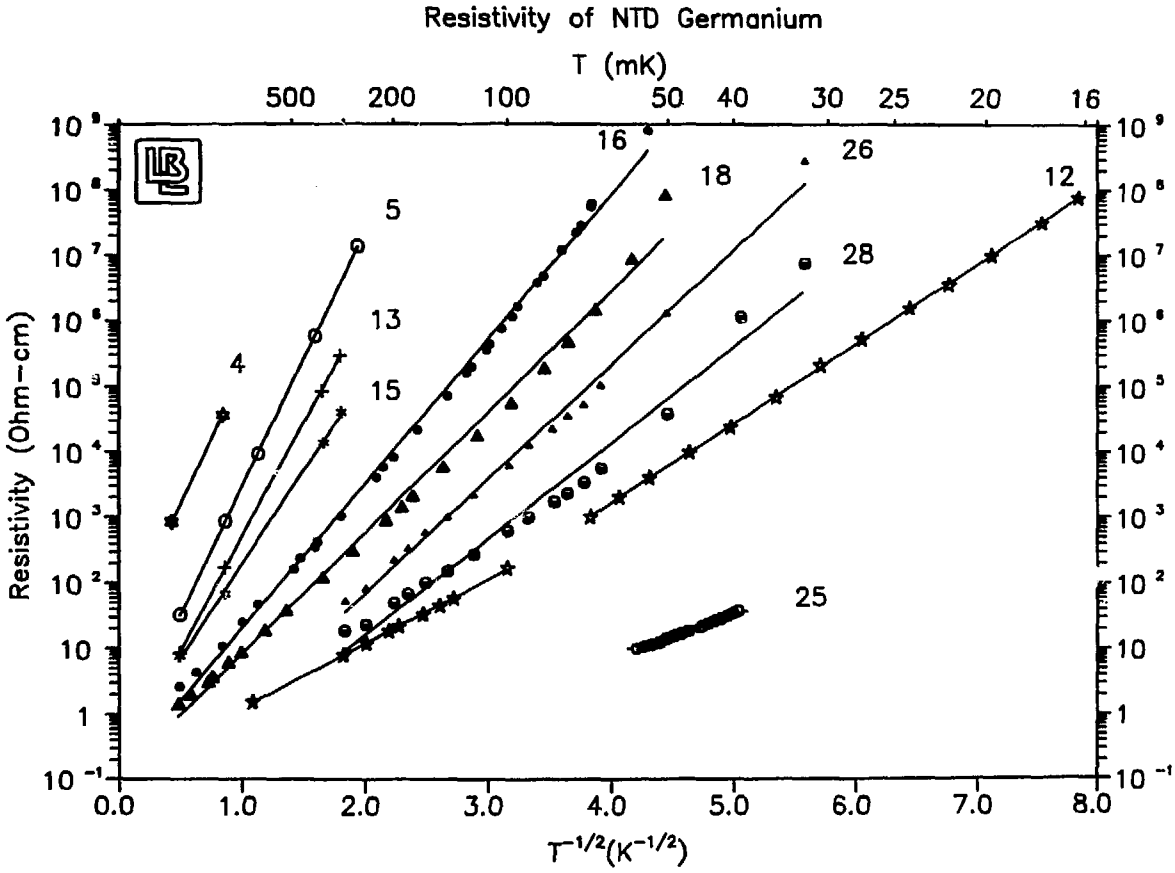
Resistivity of NTD Germanium
T (mK)
500
200
100
50
40
30
25
20
16
Resistivity (Ohm-cm)
10^{9}
10^{8}
10^{7}
10^{6}
10^{5}
10^{4}
10^{3}
10^{2}
10
1
10^{-1}
16
18
26
12
5
28
13
4
15
25
0.0
1.0
2.0
3.0
4.0
5.0
6.0
7.0
8.0
$T^{-1/2}(K^{-1/2})$
XBL 938-641

Fig. 10

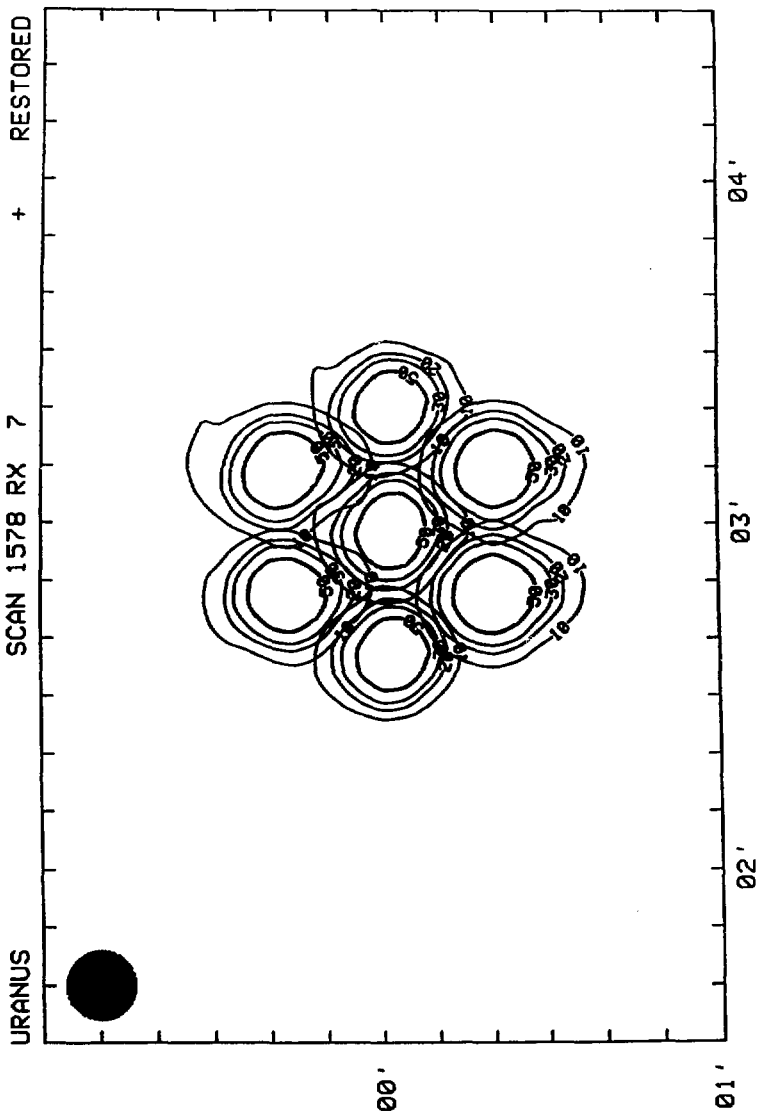

Fig. 11

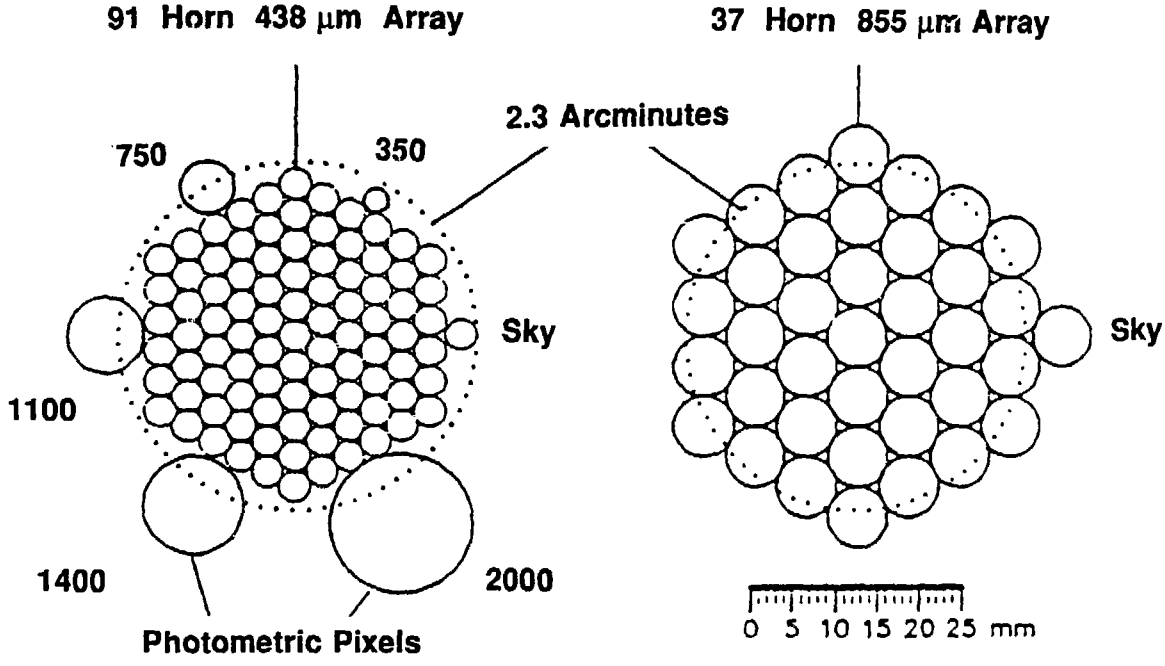

XBL 935-639

Fig. 12